Acta Crystallographica Section A
Foundations of Crystallography
ISSN 0108-7673

Received 25 August 2006
Accepted 6 November 2006

Simultaneous fitting of X-ray and neutron diffuse scattering data

D. J. Goossens,[a]* T. R. Welberry,[a] A. P. Heerdegen[a] and M. J. Gutmann[b]

[a]Research School of Chemistry, Australian National University, Canberra, ACT 0200, Australia, and [b]ISIS, Rutherford Appleton Laboratory, Chilton, Oxfordshire, OX11 0QX, UK. Correspondence e-mail: goossens@rsc.anu.edu.au

Conventional crystallographic refinement uses the Bragg-peak intensities and gives the single-site average crystal structure. Information about short-range order and local order is contained in the diffuse scattering that is distributed throughout reciprocal space. Models of the short-range order in materials can now be automatically refined. The complementarity of X-ray and neutron diffraction data, and the value of simultaneously refining a structural model against both types of data, has long been known. This paper presents the first refinement of a short-range-order model against comprehensive X-ray *and* neutron diffuse scattering data simultaneously. The sample is the organic molecular crystal benzil, $C_{14}H_{10}O_2$ (for neutron work H is replaced by D). The technique gives new insights into local order in crystalline materials, including the dynamic correlation structure indicative of the dynamics of molecules in the crystalline state, and successfully overcomes limitations of using only the X-ray data set.

1. Introduction

X-ray diffuse scattering from single crystals allows investigation of short-range order. This short-range order can be static or dynamic in nature. It may consist of ordered oxygen vacancies and cation ordering in an oxide, or molecular conformations in a molecular crystal amongst many examples (Welberry, 2004; Bürgi & Weber, 2003; Welberry, Gutmann *et al.*, 2005). The common factor is that the correlations in positions or species are not of effectively infinite range and so the scattering that results is not localized in reciprocal space.

Fitting of laboratory X-ray diffuse scattering data (Welberry *et al.*, 1998, 2001) shows that, while such data can successfully constrain the short-range correlations in the structure, they are limited in their ability to constrain the magnitudes of the thermal motions and to observe light atoms in the presence of heavier ones. Simultaneous fitting of X-ray and neutron data overcomes these limitations. The inability of an earlier study of the diffuse scattering from benzil to determine the magnitudes of thermal motions resulted from the limited reciprocal-space extent of the laboratory X-ray data (Welberry *et al.*, 2001). This can be overcome using high-energy synchrotron X-rays (Estermann & Steurer, 1998); the neutron's sensitivity to light atoms, however, cannot be replicated. This sensitivity is useful in molecular systems because (i) H atoms (or deuteriums) are common and often important in explaining the properties; and (ii) H (D) atoms are at the periphery of the molecule and undergo the greatest motions, resulting in a strong signal in the scattering *if the probe used is sensitive to these atoms*. The technique would be equally useful in oxide systems where the behaviour of the O atoms may be crucial but their scattering will be weak compared to that from heavy cations.

In the study presented here, laboratory X-ray diffuse scattering data are combined with neutron diffuse scattering data collected at a spallation source to give a detailed picture of the dynamic short-range order in the hydrogen-bonded molecular crystal benzil, $C_{14}H_{10}O_2$ (see Fig. 1). In the process, a refinement of a short-range-order model using large regions of both X-ray and neutron diffuse scattering data is performed. Above 83.5 K, the space group of benzil is $P3_121$ [$a = 8.401$, $c = 13.655$ Å, hexagonal setting (More *et al.*, 1987)]. It has been shown that deuteration changes the behaviour of benzil very little (Goossens *et al.*, 2005), hence simultaneous fitting of room-temperature X-ray data, from hydrogenous benzil (*h*-benzil), and neutron data, from *d*-benzil, is reasonable.

2. Experimental

Diffuse scattering data collection is very demanding (Estermann & Steurer, 1998; Welberry, Goossens *et al.*, 2005) as the signal covers a very wide dynamic range (typically several orders of magnitude) and the background must be very well characterized since diffuse features can be very broad and weak. In the past, analyses of diffuse scattering have usually relied on measuring small regions of reciprocal space (Sinha, 2004), but full three-dimensional (3D) modelling of the short-range order requires many reciprocal cells of data, so high-quality low-background data must be collected over a wide

expanse of reciprocal space. When collecting neutron diffuse scattering, these demands are compounded by the inherently low intensity of the neutron sources.

Crystals of *h*- and *d*-benzil were grown by controlled evaporation of solvent from a saturated acetone solution into which a seed crystal was placed. A crystal of approximately $0.5 \times 0.5 \times 2$ mm was used for X-ray data collection. A larger crystal ($5 \times 5 \times 10$ mm) was used for the neutron data collection, which was done using SXD at ISIS (Welberry *et al.*, 2003).[1] Neutrons are sensitive to inelasticity in the scattering due to their energies being comparable to phonon energies. Therefore only neutrons of energy >20 meV were used. This cut-off was determined by increasing the lower limit of the neutron energies used until the symmetry of the pattern was restored. (The intensity transfer due to the inelasticity breaks the crystallographic symmetry of the diffraction patterns.) This results in the large region of missing data in the centre of Fig. 2(*e*).

3. Modelling and refinement

The refinement procedure followed that used previously (Welberry *et al.*, 1998, 2001), with the substitution of neutron scattering lengths for X-ray scattering form factors where appropriate.

The refinement procedure uses Monte Carlo (MC) simulation to equilibrate at finite temperature a model crystal of $32 \times 32 \times 32$ unit cells subject to a set of interactions whose parameters are the parameters of the model; as unit cells cannot be considered identical, the atomic positions cannot be used as parameters. Hence in the automatic refinement the interaction parameters are refined such that they induce correlations in the model crystal which, when Fourier transformed, give a diffraction pattern containing the key features of the experimental data. Hooke's law springs (contact vectors) were used to connect molecules together and allow short-range correlations to propagate through the crystal. This results in an intermolecular energy contribution of the form

$$E_{\rm inter} = \sum_{\rm cv} F_i (d_i - d_{0i})^2, \qquad (1)$$

where d_i is the length of vector i connecting atoms on adjacent molecules, d_{0i} is its equilibrium length and F_i is its force constant. The sum is over all contact vectors (cv).

For the interactions within a molecule, three torsional angles are used, allowing the molecules to twist around the three C—C single bonds (the ϕ_i in Fig. 1). The intramolecular energy for the model is given by summing the contributions due to the deviations from the equilibrium position over all applicable angles within each molecule, summing over any cross terms (used to model interactions *between* the torsion angles), then summing over all molecules (mol). That is,

$$E_{\rm intra} = \sum_{\rm mol} \left(\sum_i F_i (\Delta\phi_i)^2 + \sum_{jk} F_{jk} \Delta\phi_j \Delta\phi_k \right), \qquad (2)$$

where in this case the F_i are the angular force constants for bond angles or dihedral angles i and the $\Delta\phi_i$ are the deviations from the equilibrium values. F_{jk} are the interaction constants for interactions between the torsion angles.

The groups within the molecules were allowed to twist around the three C—C single bonds (see ϕ_i in Fig. 1); the energy cost of these deviations was modelled through spring constant F_{12} in the previous study (Welberry *et al.*, 2001). In that study, ϕ_2 and ϕ_3 were given the same torsional spring constant as ϕ_1; here they are able to be differentiated due to the sensitivity of the neutron data to the motions of H(D) atoms at the molecular extremities. Hence in total the model contains 11 contact vector spring constants (F_1 to F_{11}), a torsional spring constant for ϕ_1 (F_{12}), one for ϕ_2 and ϕ_3 (F_{13}), a cross term for interactions between ϕ_2 and ϕ_3 (F_{14}), and a cross term for interactions between ϕ_1 and ϕ_2 and between ϕ_1 and ϕ_3 (F_{15}). (The indices number the F consecutively.)

The total energy is the sum

$$E_{\rm total} = E_{\rm inter} + E_{\rm intra}. \qquad (3)$$

At each step of the MC simulation, the energy is calculated for a single randomly selected molecule. The molecule's configuration is then randomly altered and its energy calculated again; the altered configuration is kept or rejected depending on the change in the energy. In this way, the model crystal is equilibrated, giving a configuration which depends on the set of contact vectors chosen, the values of the interaction constants, F_i, and the simulation temperature, T. The model crystal's diffraction pattern is then calculated (Butler & Welberry, 1992) and compared with the observed diffraction data. Good agreement indicates that the selected contact vectors and F_i have induced a correlation structure in the model representative of that in the real crystal.

The original fitting of the X-ray data (Welberry *et al.*, 2001) showed that the diffuse lines in the observed patterns (Fig. 2(*a*), an example is noted by a white arrow) are due to strong longitudinal correlations in the molecular positions, transmitted from molecule to molecule by a hydrogen bond between O atoms on one molecule and the *para* H atom on the next [(Welberry *et al.*, 2001), Fig. 2(*b*)]. However, the fitting used an 'overall' isotropic temperature factor, $B_{\rm overall}$, to give atomic displacement parameters (ADPs) comparable with those from single-crystal refinements (More *et al.*, 1987). The model showed how the ϕ_i within a molecule are correlated (Welberry *et al.*, 2001, Fig. 4), and arrived at an estimate for the energy of the libration of a phenyl ring (rotations around ϕ_2 and ϕ_3) of 38.0 $\rm cm^{-1}$. This compared well with *ab initio* molecular orbital calculations. However, these results were compromised by the need to use $B_{\rm overall}$, and because the torsional spring constant on ϕ_2 and ϕ_3 could not be differentiated from that on ϕ_1. Hence there is a need to refine the model using data that are a more stringent test – neutron diffraction data.

[1] Supplementary data for this paper are available from the IUCr electronic archives (Reference: LB5007). Services for accessing these data are described at the back of the journal.

Synchrotron X-ray data also offer the opportunity to collect diffuse scattering over a much wider range of scattering vector, and so would also be expected to better constrain the thermal motions than laboratory X-ray data alone. Similarly, results from single-crystal refinements can be used as constraints, and the use of results from conventional diffraction experiments and also non-diffraction-related techniques as constraints on a short-range-order model is something being explored. For organic systems, which can be deuterated, neutrons still have the advantage of being sensitive to the molecules undergoing the greatest thermal motions.

Four slices of X-ray data were used, $hk0$, $hk1$, $hk2$ and $hk\frac{1}{2}$. These extend out to approximately $\pm 4a^*$ in reciprocal space (Figs. 2*a*, *b*, *c*, *d*), with the images used being 200×200 pixels. Three slices of neutron data were used, $hk0$, $hk1$ and $hk2$. Each extended out to approximately $\pm 12a^*$ and was 400×400 pixels in size (Figs. 2*e*, *f*, *g*). A greater number of slices constrains the model further but increases the computer time required.

4. Results

Fig. 3 shows the planes of reciprocal space calculated from the final model fitted to X-ray and neutron data. These diffraction patterns can be compared directly with those in Fig. 2, and as

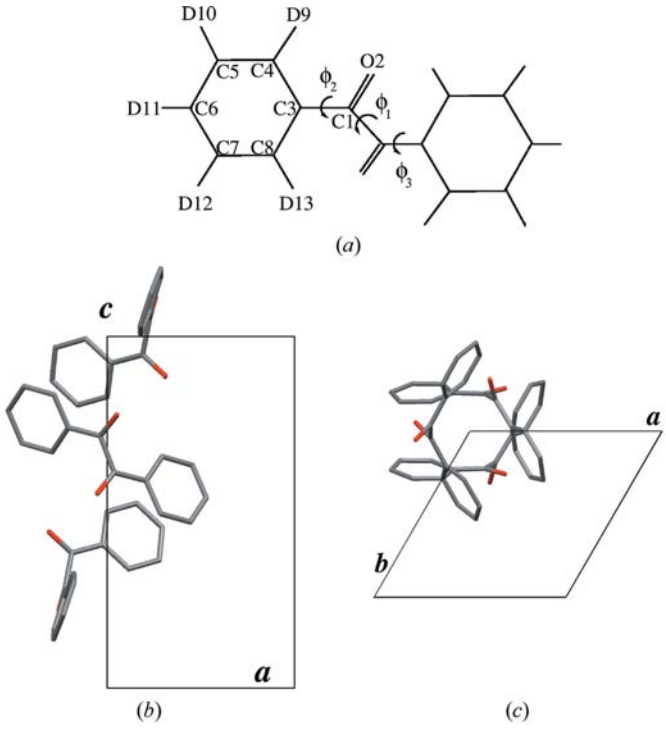

Figure 1
(*a*) Schematic diagram of the benzil molecule, with internal degrees of freedom, rotations around the torsional axes, denoted by the ϕ_is. D indicates deuterium, as deuterated benzil was used for the neutron diffraction data collection. (*b*) View of the benzil unit cell looking at the *ac* plane. Molecules can be thought of as spiralling up the *c* axis and forming three planes of molecules, each parallel with the *ab* plane. (*c*) View of the unit cell looking down the *c* axis onto the *ab* plane.

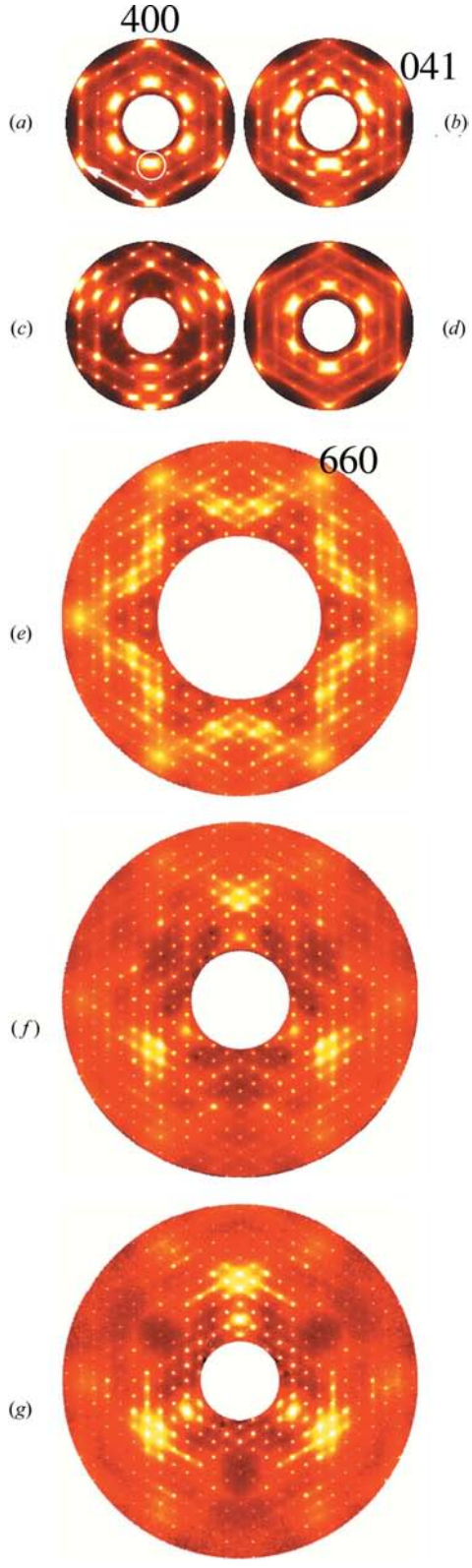

Figure 2
Observed diffuse scattering from benzil at room temperature: (*a*) gives the $hk0$, (*b*) the $hk1$, (*c*) the $hk2$ and (*d*) the $hk\frac{1}{2}$ planes measured using Co $K\alpha$ radiation. (*e*), (*f*) and (*g*) give the $hk0$, $hk1$ and $hk2$ planes measured using neutron diffraction. Arrowed lines highlight the linear features discussed in the text. Some Bragg peaks are noted to indicate the scales of the images. White gives regions of intense scattering graduating through a red palette to black which is zero intensity.

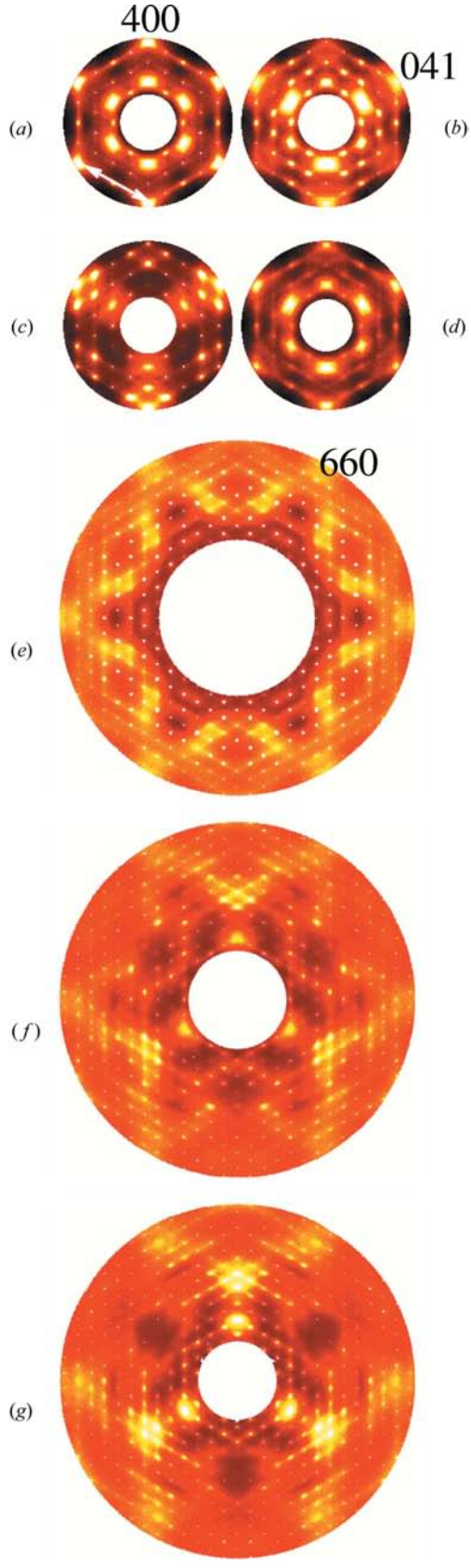

Figure 3
Calculated diffuse scattering from the model described in Table 1. (*a*) gives the *hk*0, (*b*) the *hk*1, (*c*) the *hk*2 and (*d*) the $hk\frac{1}{2}$ for X-rays. (*e*), (*f*) and (*g*) give the *hk*0, *hk*1 and *hk*2 planes for neutron scattering.

can be seen the agreement is excellent. The *R* factor is 18.8%, where

$$R = \sqrt{\frac{\chi^2}{\sum \omega I_{\rm obs}^2}}, \tag{4}$$

$$\chi^2 = \sum_{h,k,l,m} \omega_{hklm} (\Delta I)^2 \tag{5}$$

and

$$\Delta I = I_{\rm obs} - (b_m - f_m I_{\rm calc}), \tag{6}$$

where the background, b_m, and the scale factor, f_m are determined independently for each plane (m) during the χ^2 calculation and ω is a weighting. All slices of data were weighted equally. This *R* factor at first glance seems large, but the model, containing 15 parameters (two of which are zero and can be omitted), is fitting 445 841 data points, including many in the neutron data for which the statistics are poor when compared with X-ray scattering.

The large characteristic features around the Bragg peaks (an example is circled in Fig. 2*a*) are well matched, and the thin lines of scattering – really planes, as they extend up through all the observed layers – are also well reproduced. Crucially, Figs. 3(*e*), (*f*) and (*g*) demonstrate that the diffuse features are of the correct relative sizes over a wide range of scattering-vector length. This implies that the ADPs are of the correct size, which is illustrated in Fig. 4. The agreement is not perfect because the molecule here has far fewer degrees of freedom than in a conventional crystallographic fit, but plainly the scale of the ADPs is correct, as are the trends when

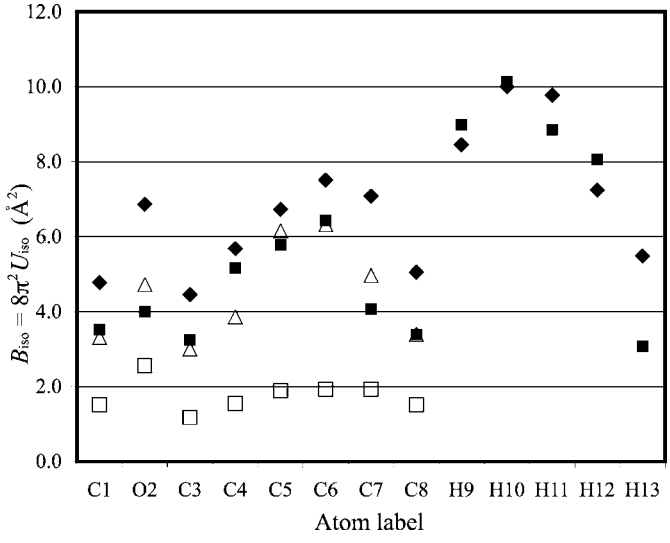

Figure 4
$B_{\rm iso}$ from the X-ray single-crystal Bragg structure (triangle, calculated from anisotropic ADPs, omitting H atoms) (More *et al.*, 1987), from neutron powder diffraction on deuterated benzil (black square, multiplied by $(300/150)^{1/2}$ as the data were collected at 150 K rather than room temperature), from the X-ray-only diffuse scattering fit (white square) *without* applying $B_{\rm overall}$ (omitting H atoms), and from the combined fit to X-ray and neutron diffuse data (black diamond). Labels on the horizontal axis accord with those shown in Fig. 1, with hydrogen and deuterium being considered as equivalent.

Table 1
Spring constants in units of k_BT from the final combined X-ray and neutron model (X+N, averaged over eight cycles of refinement after the model had converged; uncertainties were also calculated from these cycles), compared with those from the X-ray-only study [X, *cf.* Model 2 from Table 3 in Welberry *et al.* (2001)].

Num. is the number of each type of interaction associated with each molecule. Ratio X/(X+N) gives the ratios of the spring constants from the two models.

Parameter	Num.	X	X+N	Ratio X/(X+N)
F_1	4	120.0	3.90 (6)	31
F_2	4	48.6	1.20 (9)	40
F_3	4	15.7	0.25 (9)	63
F_4	4	85.7	4.4 (3)	19
F_5	4	34.8	0.67 (9)	52
F_6	2	16.5	0.82 (3)	20
F_7	4	145.6	2.11 (3)	69
F_8	2	76.8	2.11 (6)	36
F_9	4	120.4	4.1 (7)	29
F_{10}	2	80.3	2.9 (1)	28
F_{11}	4	37.8	1.40 (9)	27
F_{12}	1	0.159	0.000 (1)	N/A
F_{13}	2	0.159	0.140 (3)	1.1
F_{14}	1	0.000	0.000 (1)	N/A
F_{15}	2	0.000	0.0067 (5)	0.0

compared with X-ray single-crystal and neutron powder diffraction results. The results from the X-ray-diffuse-only model show the B_{iso}s *without* the contribution of $B_{overall}$ (~ 6.17 Å^2). The trend with atom is correct (even if too weak) but the magnitudes are not acceptable (H atoms omitted from X-ray results). It can be seen that the combined neutron + X-ray model provides a much better fit both in magnitude and in the trends exhibited by the values. Full anisotropic ADPs are available from diffuse scattering; B_{iso} values are listed for conciseness.

5. Discussion

The final set of refined intermolecular spring constants from the combined fit, F_1 to F_{11}, are listed in Table 1 (*cf.* Welberry *et al.*, 2001, Table 3). The constants are all greatly scaled down relative to the earlier model (on average by a factor of ~ 38), which allows the greater thermal motion to occur, but the same springs have remained relatively strong or weak, indicating that the correlation structure produced by the X-ray modelling is essentially intact. The major exception is that F_4 is relatively stronger (scaled down by a factor of ~ 19) in the combined fit while F_7 has become much weaker (scaled down by a factor of 69). All contact vectors but 4 and 7 act either within the *ab* plane (1, 2 and 11) or along the *c* axis (3, 5, 6, 8, 9 and 10). Overall, the combined significance of 4 and 7 is little changed; indeed the balance between the contributions of the three groups of contact vectors ('*ab*', '*c*' and '4 and 7') to the molecular energy is almost the same here as in the X-ray work. Hence the X-ray data were capable of determining the relative importance of the intermolecular interactions, but not capable of determining their magnitudes.

Fig. 2(*e*) shows that the neutron data close to the origin of reciprocal space are absent due to the strong inelastic effects seen there (Welberry *et al.*, 2003). This is where the planes of scattering that lie perpendicular to the *hk*0 plane (see for example the arrow in Fig. 2*a*) are most pronounced. It was found that refining the model against neutron data only resulted in a reduction in the strong longitudinal correlations in the molecular positions as transmitted by hydrogen bonding between the O atoms of one molecule and the *para* H atom on the next. This meant that, when the model refined purely against neutron data was used to predict the X-ray diffuse scattering, the planes of scattering as seen in Figs. 2(*a*), (*b*), (*c*) and (*d*) were almost entirely absent. This suggests that the excellent statistics and resolution of the X-ray experiment and its ability to measure close to the origin of reciprocal space means it is a stronger constraint on the longer-ranged correlations, while the large reciprocal-space coverage of the neutron data complements this by more strongly constraining the thermal motions.

The energetics of the internal molecular motions were re-examined in the light of this more quantitative model. The spring constant on ϕ_2 and ϕ_3 suggests that the energy of the phenyl group twisting is 35.3 ± 0.2 cm^{-1}, in very close agreement with the result in the previous study (38 cm^{-1}), which was itself in good agreement with *ab initio* results for an isolated molecule and with experimental Raman measurements (Hanuza *et al.*, 2004). This indicates that the torsional vibrations of the phenyl rings are not strongly altered by the crystal environment. The same *ab initio* calculation showed that the lowest mode of vibration was a twisting around the centre bond – corresponding to ϕ_1. This is indeed found to be the case here, where F_{12} and F_{13} are well differentiated, with F_{12} being effectively zero; unlike when fitting the X-ray data alone, fixing $F_{12} = F_{13}$ degraded the fit substantially, with the

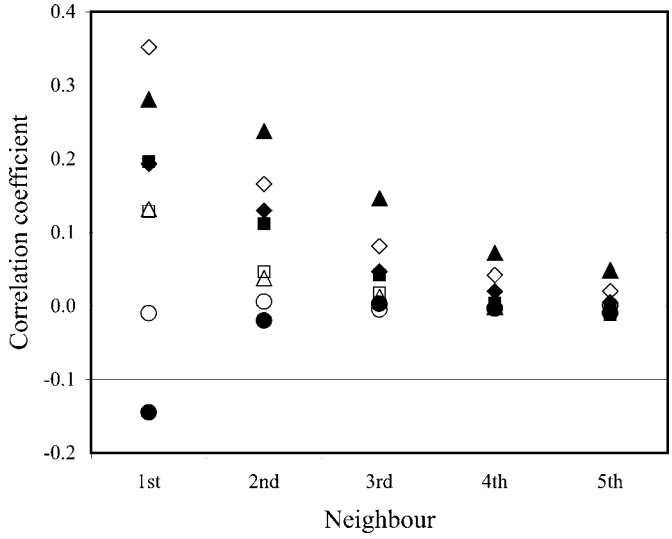

Figure 5
Some short-range correlations in benzil as revealed by diffuse scattering. Hollow symbols apply to neighbours in the *a* direction while filled apply to neighbours along the *c* axis. Diamonds show correlations between *a*-direction displacements of neighbours, triangles give correlations between *c*-direction displacements while squares give *y*-direction displacements, where *y* completes a Cartesian set of coordinates. Circles give correlations in the values of ϕ_1 on neighbouring molecules.

best R factor being 22.2% when $F_{12} = F_{13}$. The $B_{\rm overall}$ in Welberry *et al.* (2001) contributed an uncorrelated global displacement to the whole molecule so could not compensate for any internal motions. Hence the spring constants on ϕ_2 and ϕ_3 remain little changed, and give much the same estimate for the energy of the phenyl libration. Of the cross terms, F_{14} is also effectively zero while F_{15} was found to be small but positive, indicating a negative correlation between deviations in ϕ_1 and the other angles. In reality there is not a 'zero-energy' mode around the central bond, because (i) molecular motions are inhibited by the intermolecular interactions and (ii) interaction between ϕ_1 and the other angles is not zero.

The model's structure was examined to gain insight into the real crystal. Fig. 5 shows correlations in displacements as a function of neighbour. A positive correlation indicates that displacements are parallel, such that the correlated molecules will tend to maintain their separation. The plot shows that displacements in the direction of the vector connecting neighbours tend to be stronger (diamond and filled triangle) while those perpendicular are weaker. It also shows that $\Delta\phi_1$ is negatively correlated for molecules adjacent along the *c* axis, which is to say $\Delta\phi_1$ tends to be of opposite sign for molecules adjacent along the *c* axis, while it is uncorrelated for neighbours in the *a* direction (and in the *hk* plane generally). Other correlations (not plotted) show that the cross correlations between displacements (for example between *a*-direction displacements on a molecule and the *c*-direction displacements on its neighbour) are weak, as are correlations between ϕ_2 and ϕ_3 on neighbours and cross correlations between the torsional angles within a molecule.

6. Conclusions

A simultaneous fitting of a 3D short-range-order model to large areas of X-ray *and* neutron diffuse scattering data has been performed. Using the neutron data, the fit was able to differentiate the torsional spring constants on molecular torsional degrees of freedom, owing to the sensitivity of neutrons to the atoms at the molecular extremities (H/D) and the greater extent in reciprocal space of the neutron data. This also better constrained the atomic displacement parameters of the model. The final model agreed broadly with the correlation structure determined from the previous X-ray refinement.

The short-range dynamic correlation structure was revealed, showing how the conformation of a molecule influences its neighbours. Information on how the crystalline environment affects molecular conformation can lead to a better understanding of polymorphism, significant in the pharmaceutical industry. Hence this technique offers a powerful new way to explore the dynamics and short-range order within solids, including pharmaceuticals and, potentially, large biomolecules, as it gives a model of how the molecules interact and how their configurations propagate. For other types of systems, such as substituted oxides, better understanding of short-range order offers new opportunities to tune a material's properties and optimize its technological usefulness.

The support of the Access to Major Research Facilities Program, the Australian Partnership for Advanced Computing and of the Australian Research Council is gratefully acknowledged. W. I. F. David contributed to earlier studies and helped enable this work.

References

Bürgi, H.-B. & Weber, T. (2003). *Mol. Cryst. Liquid Cryst.*, **390**, 1–4.
Butler, B. D. & Welberry, T. R. (1992). *J. Appl. Cryst.* **25**, 391–399.
Estermann, M. A. & Steurer, W. (1998). *Phase Transit.* **67**, 165–195.
Goossens, D. J., Wu, X. & Prior, M. (2005). *Solid State Commun.* **136**, 543.
Hanuza, J., Sąsiadek, W., Kucharska, E., Michalski, J., Mączka, M., Kaminskii, A. A., Koronienko, A. A., Dunina, E. B., Klapper, H., Hulliger, J. & Mohmed, A. F. A. (2004). *J. Raman. Spect.* **35**, 224–235.
More, M., Odou, G. & Lefebvre, J. (1987). *Acta Cryst.* B**43**, 398–405.
Sinha, S. K. (2004). *Z. Kristallogr.* **219**, 143–147.
Welberry, T. R. (2004). *Diffuse X-ray Scattering and Models of Disorder.* Oxford University Press.
Welberry, T. R., Goossens, D. J., David, W. I. F., Gutmann, M. J., Bull, M. J. & Heerdegen, A. P. (2003). *J. Appl. Cryst.* **36**, 1440–1447.
Welberry, T. R., Goossens, D. J., Edwards, A. J. & David, W. I. F. (2001). *Acta Cryst.* A**57**, 101–109.
Welberry, T. R., Goossens, D. J., Heerdegen, A. P. & Lee, P. L. (2005). *Z. Kristallogr.* **220**, 1052–1058.
Welberry, T. R., Gutmann, M. J., Woo, H., Goossens, D. J., Xu, G., Stock, C., Chen, W. & Ye, Z.-G. (2005). *J. Appl. Cryst.* **38**, 639–647.
Welberry, T. R., Proffen, T. & Bown, M. (1998). *Acta Cryst.* A**54**, 661–674.